Scission of 2D Inorganic Nanosheets via Physical Adsorption on a Nonflat Surface

Nobuyuki Sakai, Masahiko Suzuki, and Takayoshi Sasaki*

N. Sakai, T. Sasaki
International Center for Materials Nanoarchitectonics (WPI-MANA), National Institute for Materials Science (NIMS), 1-1 Namiki, Tsukuba, Ibaraki 305-0044, Japan
E-mail: sakai.nobuyuki@nims.go.jp

M. Suzuki
Research Center for Advanced Measurement and Characterization, National Institute for Materials Science (NIMS), 1-2-1 Sengen, Tsukuba, Ibaraki 305-0047, Japan

Keywords: 2D materials, secondary processing, intermolecular forces, tensile stress, crevices

Secondary processing of 2D nanosheets is an important technique for fabrication of devices and modulation of properties. However, methods for the secondary processing have not been well developed yet, particularly for the scission along crystallographic orientation. In the present paper, it is reported that titania nanosheets can be orthogonally sectioned into substantially rectangular-shaped fragments when deposited on a nonflat substrate surface via spin-coating their suspension. Such events occur for all the nanosheets on the substrate surface. In the deposition process, nanosheets float and stay flat on top of the solvent surface, and adsorb on the substrate with conforming to the bumpy surface by following the descending solvent level. Because the nanosheet area is smaller than the actual area of the bumpy surface having the same projected area, the nanosheet experiences tensile stress along its lateral direction. The tensile stress originates from the intermolecular forces acting between the nanosheet and the substrate surface upon the adsorption on the substrate. Due to the high 2D anisotropy, the integrated intermolecular forces can be large enough to cleave the chemical bonds, leading to the scission of the nanosheet. This interesting finding may offer a new processing technique for cutting and shaping various 2D materials.

1. Introduction

2D materials or nanosheets have been extensively studied in the last several decades and a wide range of nanosheets, such as graphene, hexagonal boron nitride, transition metal

chalcogenides, black phosphorus, metal oxides, layered double hydroxides, and MXenes, have been synthesized via exfoliation of their mother layered compound into single layers.[1–7] The nanosheets exhibit various fascinating properties depending on their structure and composition.

Secondary processing of 2D nanosheets is an important technique for modulation of properties as well as fabrication of devices. The drilling of graphene via O_2 plasma treatment[8] or helium ion beam milling[9] has been reported to obtain graphene nanomesh, yielding semiconducting nature. The scission of 2D materials, such as graphene,[10,11] MoS_2,[12] and WSe_2,[13,14] has been conducted during the process of so-called tear-and-stack technique to form twisted bilayer 2D materials, showing interesting properties.[15] The cleavage of 2D materials has also often been reported in studies examining their mechanical properties. For example, graphene[16–18] and reduced graphene oxide[19] adsorbed on a substrate can be torn when the substrate is mechanically pulled along the lateral direction, while various types of 2D nanosheets are wrinkled or crumpled upon mechanical compression.[20–25]

The scission of 2D nanosheets along crystallographic orientation is also important for controlling the size and shape of the sectioned nanosheets. It has been reported that the fragmentation of nanosheets occurs when they experience vigorous agitation[26] or ultrasonic treatment[27] in their suspension, although the cleavage direction is uncontrollable, yielding irregular size and shape. Scanning probe lithography[28–30] and femtosecond laser micromachining[31] have been applied for cutting and shaping the 2D nanosheets. For the scission along crystallographic direction by these processes, however, it is necessary to examine the crystal orientation of the nanosheet in advance. Since it is difficult to examine the crystal orientation of 2D nanosheets deposited on a substrate, the scission along crystal orientation has not been achieved, to date, to the best of our knowledge.

In the present study, we have examined if the scission of 2D nanosheets along crystallographic orientation can be driven by intermolecular forces acting between the nanosheets and a substrate surface. The scission of nanosheets is achieved via the dissociation of chemical bonds inside the nanosheets. The magnitude of intermolecular forces is several to several tens of kilojoules per mole, which is much smaller than the bond dissociation energy (several hundred kilojoules per mole).[32] However, when a 2D nanosheet adsorbs on a substrate, the total intermolecular force acting between the nanosheet and the substrate may surpass the total bond dissociation energy required to section the nanosheet along one lateral direction. Because the number of atoms existing in the thickness direction is constant and

small for the nanosheets, the number of chemical bonds across one lattice plane perpendicular to the lateral direction of the nanosheets linearly increases, as the lateral size of nanosheets expands. In contrast, the total intermolecular force quadratically increases, because it depends on the contact area to the substrate. Hence, the total intermolecular force will exceed the total dissociation energy of chemical bonds across the vertical lattice plane of nanosheets when the aspect ratio (lateral size/thickness) of nanosheets is a certain value or greater. In other words, the aspect ratio of 2D nanosheets is one key factor for realizing their scission by the integrated intermolecular forces.

Among various types of 2D nanosheets, the titania nanosheet is one of the most studied and characterized (Figure S1, Supporting Information)[33–37] and has a uniform crystallographic thickness of 0.75 nm including the outer edge of surface oxygen atoms.[38] The lateral size reaches to several tens of micrometers, leading to a very large aspect ratio of up to several tens of thousands. The titania nanosheets are obtained as colloidal 2D crystals monodispersed in solutions, and they can be deposited as separated individual unilamellar entities on a substrate surface through various solution processes such as electrostatic self-assembly and Langmuir–Blodgett deposition.[39,40] In addition, we have recently achieved a neat monolayer tiling of the titania nanosheets via a facile spin-coating method.[41] Hence, the titania nanosheets are the most suitable material for examining the possibility of the dissociation of chemical bonds by the intermolecular forces acting on the substrate.

As will be presented below, the titania nanosheet can be sectioned when physically adsorbed on a nonflat surface, which was confirmed by the formation of crevices running within the nanosheets. The crevices tended to be orthogonal to each other and perpendicular to the edge of the rectangle-shaped nanosheet, indicating the scission along crystallographic direction with reflecting the 2D rectangular lattice of the titania nanosheets.

2. Results and Discussion

The titania ($Ti_{0.87}O_2^{0.52-}$) nanosheets were synthesized via exfoliation of the lepidocrocite-type layered titanate through well-established process (Figure S1, Supporting Information).[33,34,37] Details of the procedure are described in Experimental Section. The prepared $Ti_{0.87}O_2^{0.52-}$ nanosheets were deposited on a silicon substrate by spin-coating their colloidal suspension in dimethyl sulfoxide (DMSO).[41] As observed by atomic force microscopy (AFM), the $Ti_{0.87}O_2^{0.52-}$ nanosheets were laterally assembled into a neatly tiled monolayer on a silicon substrate, except for small overlapping areas between neighboring nanosheets (**Figure 1**a). The observed thickness of the nanosheets was 1.2 nm and uniform

within a single nanosheet as well as between different nanosheets, indicating their unilamellar nature. The discrepancy from the crystallographic thickness of 0.75 nm is due to adsorption of water molecules on both sides of the nanosheets, as discussed in our previous paper.[42] It is considered that the DMSO molecules used to prepare the film can evaporate, and be replaced with water molecules derived from the surrounding air. On the other hand, the lateral size varied in the range of 10–20 μm according to the crystal size of the mother layered titanate. The aspect ratio (lateral size/crystallographic thickness) is as large as 13000–26000. As determined by in-plane X-ray diffraction (XRD) measurements (Figure 1b), the 2D structure of $Ti_{0.87}O_2^{0.52-}$ nanosheets was characterized by a face-centered rectangular unit cell of a = 0.37864(4) nm and c = 0.29833(2) nm (Figure 1c), retaining the host layer architecture of mother layered titanate (Figure S1, Supporting Information), which is consistent with our previous reports.[42–44]

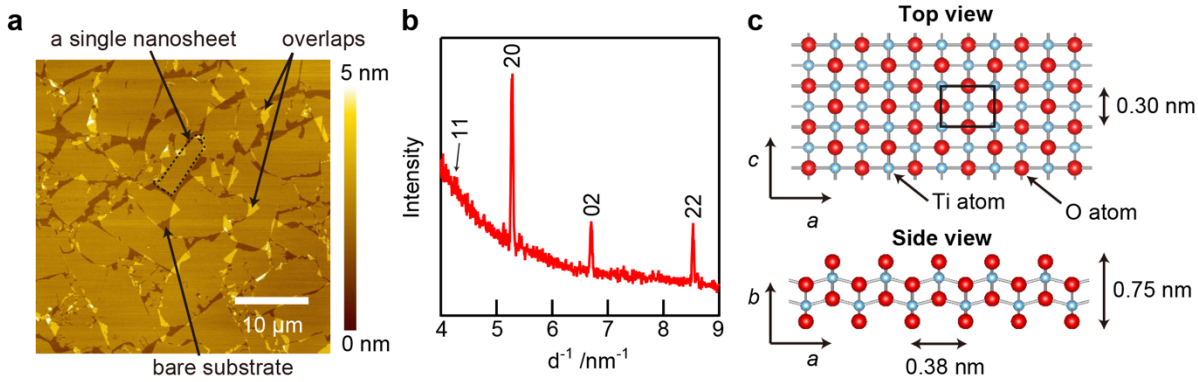

Figure 1. a) An AFM image of $Ti_{0.87}O_2^{0.52-}$ nanosheets adsorbed on an Si wafer and b) their in-plane XRD pattern. c) Schematic illustration of the atomic architecture of $Ti_{0.87}O_2^{0.52-}$ nanosheets. The unit cell is designated with a rectangle shown in the image (Top view).

The neat monolayer tiling of $Ti_{0.87}O_2^{0.52-}$ nanosheets prepared via the spin-coating method can be also observed by scanning electron microscopy (SEM). The shape of the nanosheets was clearly recognized when a polished conductive indium tin oxide (ITO) substrate with a relatively flat surface was employed, owing to different emission abilities of secondary electrons between $Ti_{0.87}O_2^{0.52-}$ nanosheets and ITO. The image was composed of white, gray, and dark gray parts, corresponding to the bare ITO substrate, the monolayer of the nanosheets, and their overlapped area (**Figure 2**a), respectively, which is consistent with the AFM image shown above (Figure 1a). Even when the nanosheets were spin-coated on an unpolished ITO substrate with a bumpy surface, the monolayer tiling of nanosheets was attained (Figure 2d,e).

It was surprising to find that numerous crevices were formed within each nanosheet and the nanosheets were sectioned into smaller pieces (Figure 2d–f). Such events were observed for all the nanosheets on the substrate surface. The crevices running within a nanosheet tend to be perpendicular to the edge of the nanosheet and orthogonal to each other at their intersections (Figure 2f). It is worth mentioning that the sectioned nanosheets within the originally single nanosheet are aligned along the same crystal orientation with gaps between them (Figure 2e). The width of the crevices was 75–170 nm at the widest (designated by arrows) and thinner crevices were also observed in the area surrounded by the wider crevices, as shown by a magnified SEM image (Figure 2f). Since no such crevices were observed when the nanosheets were adsorbed on the polished flat ITO surfaces (Figure 2a–c), it is considered that the bumpy surface of the unpolished ITO substrate is responsible for the formation of crevices within the nanosheets.

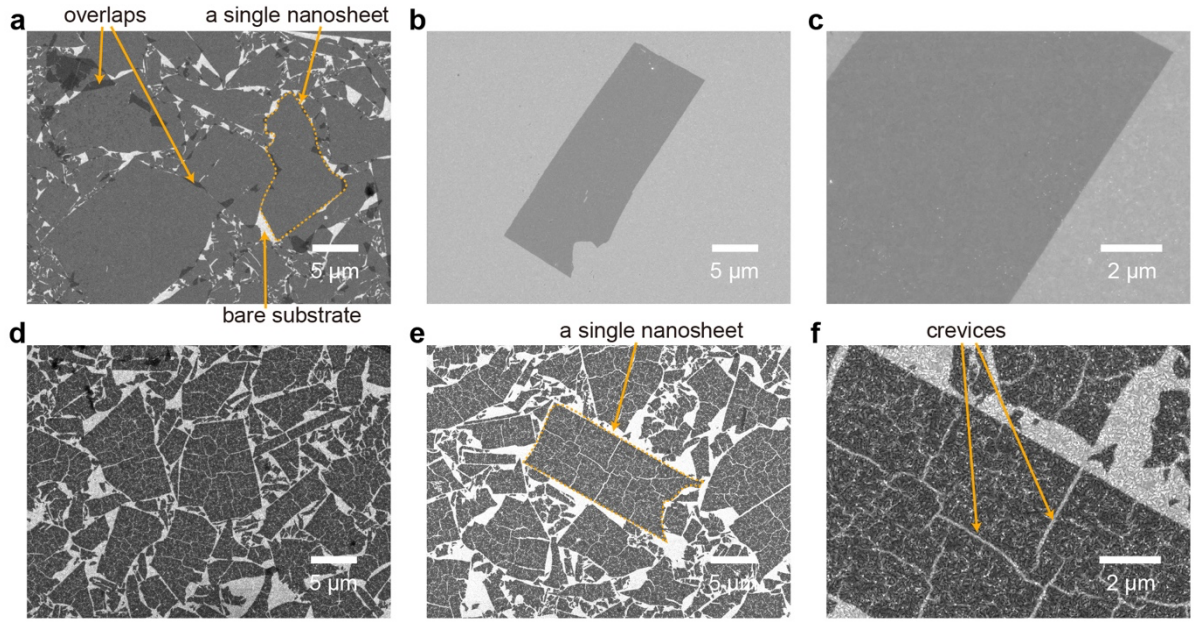

Figure 2. SEM images of $Ti_{0.87}O_2^{0.52-}$ nanosheets spin-coated on ITO substrates with a–c) polished flat and d–f) unpolished bumpy surfaces. c,f) Magnified images of a part of the nanosheet shown in the center of the images (b,e), respectively.

Then, we examined the surface morphology of the two types of ITO substrates used above (polished and unpolished) by AFM observation. The bare polished ITO surface showed a relatively flat morphology with surface roughness (*Ra*) of *Ra* = 0.38 nm (**Figure 3**e, red line), although the surface had many polishing marks (Figure 3a). In contrast, the bare unpolished ITO surface yielded an *Ra* value of 5.0 nm (Figure 3c), showing a bumpy surface composed

of ITO particles with a lateral dimension of ≈100 nm and a height of ≈20 nm (Figure 3e, blue line). We also observed the ITO surfaces coated with the neat monolayer tiling of $Ti_{0.87}O_2^{0.52-}$ nanosheets. The shape of the nanosheets adsorbed on the polished ITO surface could be recognized owing to its relatively flat surface (Figure 3b), whereas the shape of the nanosheets was hardly recognized when adsorbed on the unpolished ITO surface (Figure 3d). It is worth mentioning that there were no significant differences in the cross-sectional profile or *Ra* values between the unpolished ITO surfaces with and without the adsorption of the nanosheets (Figure 3e, green and blue lines), suggesting that the nanosheets were adsorbed on the unpolished ITO substrate with conforming to its bumpy surface. This is consistent with our previous results that the titania nanosheets are highly flexible in the thickness direction[45] and can be adsorbed along the non-flat morphology of the substrate surfaces.[46,47]

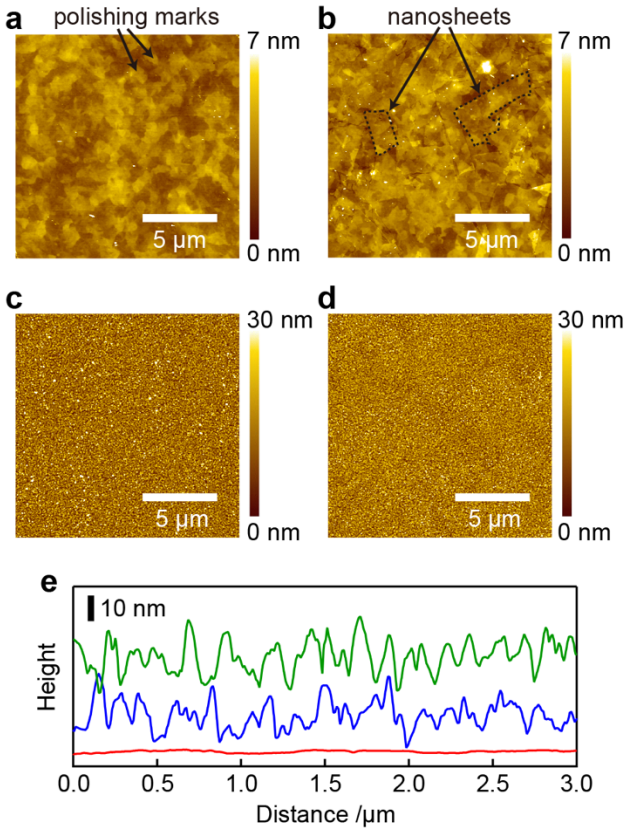

Figure 3. AFM images of a,b) polished and c,d) unpolished ITO surfaces a,c) without and b,d) with the adsorption of the neat monolayer tiling of $Ti_{0.87}O_2^{0.52-}$ nanosheets. e) Cross sectional profiles of bare polished ITO surfaces (red line, *Ra* = 0.38 nm), bare unpolished ITO surfaces (blue line, *Ra* = 5.0 nm), and unpolished ITO surfaces adsorbed with $Ti_{0.87}O_2^{0.52-}$ nanosheets (green line, *Ra* = 5.0 nm).

We discuss the mechanism by which the observed crevices within each nanosheet are formed when adsorbed on a non-flat surface (**Figure 4**). According to the observed cross sectional profile (Figure 3e, blue line), we model the bumpy surface of unpolished ITO substrates as continuous mountains with a height of 20 nm at a repeating distance of summits of 100 nm. In the adsorption process via the spin-coating, the nanosheets tend to float on a very thin solvent layer covering the substrate surface owing to amphiphilic nature of tetrabutylammonium (TBA) ions adsorbed on the nanosheets (Figure 4, i).[48,49] As the solvent gradually evaporates, the nanosheets approach to the substrate surface with staying flat and many parts of a single nanosheet contact multiple summits of the substrate surface, and begin to adsorb with conforming to the bumpy surface at each location. This is because the nanosheet attempts to follow the descending solvent level in between the adsorbed points due to surface tension working at the nanosheet/solvent interface (Figure 4, ii). During this process, the nanosheet experiences tensile stress along its lateral direction between the neighboring adsorbed points because the area of the nanosheet is smaller than the actual area of the non-flat substrate surface having the same projected area. The adsorption of the nanosheet on the substrate surface is the origin of the tensile stress, which can be estimated by adhesion energies based on the intermolecular forces as described later. As the contact area increases due to further evaporation of the solvent, the tensile stress also increases to tear the nanosheet in the middle between the adsorbed points (Figure 4, iii). Finally, a part of the nanosheet remaining on the solvent surface adsorbs on the substrate when the solvent becomes completely dried, and nanosheets separated by many crevices running within the original single nanosheet are remained on the substrate surface (Figure 4, iv), as observed by SEM (Figure 2d–f).

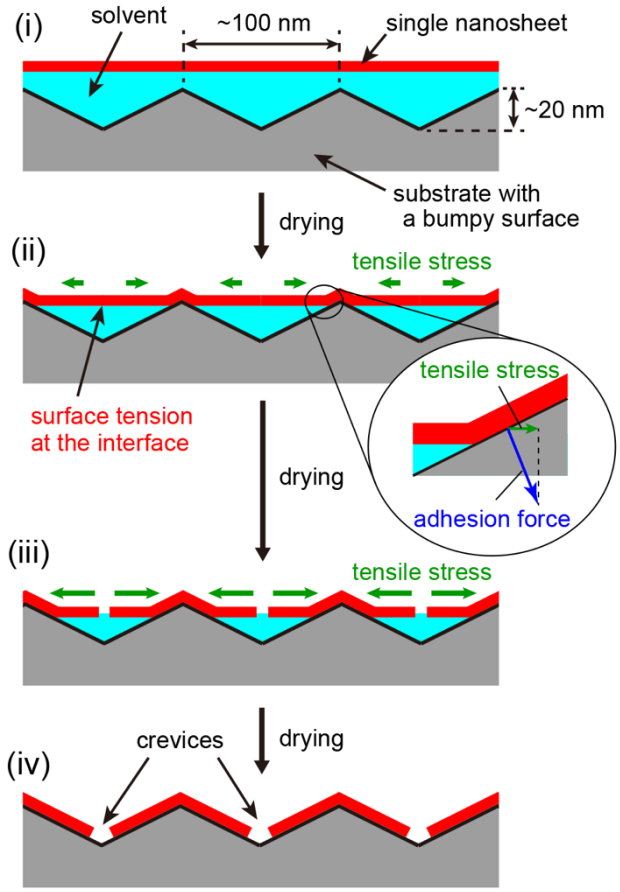

Figure 4. Schematic illustration of plausible mechanism for the scission of nanosheets upon adsorption on substrates with a non-flat surface. See the text for details.

In the discussion above, the integrated intermolecular forces need to be large enough to hold the nanosheets onto the substrate surface, yielding the tensile stress for the scission of nanosheets. If the integrated intermolecular forces are weaker than the total dissociation energy of chemical bonds across one lattice plane perpendicular to the lateral direction of the nanosheet, the nanosheet would slide on the substrate and conform to the bumpy surface of substrate to release the tensile stress, and hence the nanosheet will not be sectioned. To examine the threshold of the nanosheet size where the integrated intermolecular forces exceed the total dissociation energy of chemical bonds across the vertical lattice plane of the nanosheet for the scission along one lateral axis, we calculate the intermolecular forces and the bond dissociation energies as a function of the lateral size of the nanosheets. For the comparison, we assume that the nanosheet shape is rectangular (ratio of long side to short side is 0.38/0.30) similar to its unit cell shape,[50] and that the nanosheet splits along each axis into two parts of identical shape (**Figure 5**, inset). The intermolecular forces can be estimated as the adhesion energy (Γ) between the $Ti_{0.87}O_2^{0.52-}$ nanosheet and the ITO surface, which can be

calculated by $\Gamma = 2\ (\gamma_{TNS} \times \gamma_{ITO})^{1/2}$ based on the surface free energies of the $Ti_{0.87}O_2^{0.52-}$ nanosheet (γ_{TNS}) and ITO surface (γ_{ITO}).[51] The surface free energies of the solid are calculated by **Equation (1)** on the basis of contact angle measurements of two types of liquids on the solid:

$$(1 + cos\theta)\gamma_L = 2(\gamma_S^d\ \gamma_L^d)^{1/2} + 2(\gamma_S^h\ \gamma_L^h)^{1/2} \quad (1)$$

where θ is the contact angle, γ_L and γ_S are the surface free energies of the liquid and solid, respectively, and the superscripts *d* and *h* refer to the dispersion force and hydrogen bonding components of the surface free energy, respectively.[52] We carried out the contact angle measurements for the $Ti_{0.87}O_2^{0.52-}$ nanosheet and unpolished ITO surfaces (**Table 1**), and the surface free energies were obtained as γ_{TNS} = 73.4 mJ/m^2 and γ_{ITO} = 74.7 mJ/m^2 according to Equation 1. Then, the adhesion energy was determined to be Γ = 148 mJ/m^2, which corresponds to 5.1 kJ/mol of $Ti_{0.87}O_2^{0.52-}$. This value is comparable to the magnitude of the intermolecular forces reported,[32] indicating that the $Ti_{0.87}O_2^{0.52-}$ nanosheets are physically adsorbed on the ITO surface. This is reasonable because the chemical bonds of the nanosheets are terminated on their surface perpendicular to the sheet normal (Figure 1c). When the nanosheets adsorb on the ITO surface during the spin-coating, the interface between the nanosheet and the ITO surface is produced by replacing with the interface between the nanosheet and DMSO in the suspension. The adhesion energy between the nanosheet and DMSO is calculated to be 113 mJ/m^2 using the surface free energy of DMSO (43.5 mJ/m^2).[53] Hence, the difference of the adhesion energy, 35 mJ/m^2, can be used for the scission of the nanosheets. Since the adhesion force works perpendicular to the interface plane, the tensile stress working on the nanosheet in the lateral direction can be calculated as $\Gamma \times \sin\theta$ according to the morphology model of the bumpy ITO surface (see Figure 4, $\theta = \tan^{-1}(0.4)$). On the other hand, the binding energy of Ti–O bonds is reported to be ~670 kJ/mol.[54] According to the crystal structure of the $Ti_{0.87}O_2^{0.52-}$ nanosheets (Figure 1c), the number of Ti–O bonds across each vertical lattice plane is 2, 4, and 6 along the [01], [10], [11] axes within the unit cell size (0.38 nm × 0.30 nm), corresponding to 6.67, 10.5, and 12.4 nm^{-1}, respectively, assuming that the vacancies at the Ti site of the $Ti_{0.87}O_2^{0.52-}$ nanosheet are fully occupied with Ti atoms. It is noted that the total dissociation energy required to section the nanosheet corresponds to the energy difference between the original nanosheet and the sectioned nanosheets with dangling bonds formed at the edge along the crevice, although the formed dangling bonds would be stabilized by the subsequent processes such as reconstruction of the edge structure and/or adsorption of molecules existing in the ambient atmosphere. To estimate the threshold of the nanosheet size required to section the nanosheet, the adhesion energy

working as tensile stress in the lateral direction as well as the dissociation energy of the Ti–O bonds across each lattice plane are plotted against the nanosheet size (Figure 5). The length of short side ([01] axis) of the rectangle is used as the nanosheet size. When the lateral size of 2D materials expands, the dissociation energy of chemical bonds required to section the nanosheet along each axis linearly increases while the intermolecular force quadratically increases, as shown in Figure 5. Hence, the total intermolecular force exceeds the total dissociation energy of chemical bonds across one vertical lattice plane of 2D materials when the aspect ratio of 2D materials is a certain value or greater. We found that the adhesion energy exceeds the dissociation energy when the lateral size is larger than 450 nm and 900 nm if crevices run along the [01] and [10] axes of the nanosheet, respectively. The threshold for the crevices along the [11] axis is 1350 nm, which is larger than that along the [01] and [10] axes, depending on the density of Ti–O bonds. Since the local minimum in the density of Ti–O bonds that needs to be cleaved was found for that along [01] or [10] axis among all the directions (Figure S2, Supporting Information), it is suggested that the crevices are likely to occur along the [01] or [10] axis of the nanosheet. Hence, the orthogonal crevices appear as a result of the formation of crevices running along the [01] or [10] axes of the $Ti_{0.87}O_2^{0.52-}$ nanosheet.

Table 1. Contact angles for water and methylene iodide on the $Ti_{0.87}O_2^{0.52-}$ nanosheet and unpolished ITO surface and their surface free energies.

	Contact angle (degree)		Surface free energy (mJ/m^2)[a]		
	Water	Methylene iodide	γ_S^d	γ_S^h	γ_S
$Ti_{0.87}O_2^{0.52-}$ nanosheet	3.4 ± 0.6	38.1 ± 0.7	28.8	44.6	73.4
ITO surface	3.5 ± 0.4	25.2 ± 2.2	34.2	40.5	74.7

[a] γ_S is the surface free energy of the solid, and the superscripts *d* and *h* refer to the dispersion force and hydrogen bonding components, respectively.

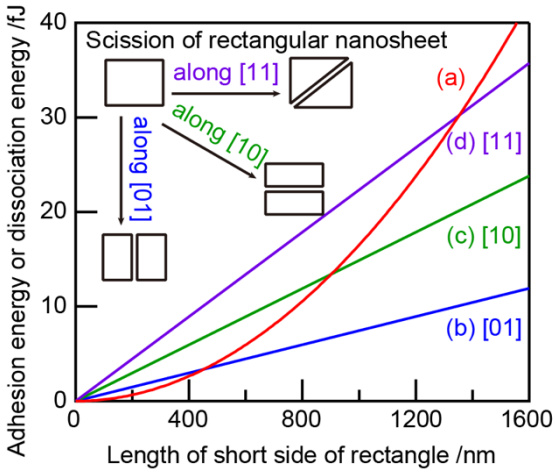

Figure 5. Calculated adhesion energy upon adsorption of the $Ti_{0.87}O_2^{0.52-}$ nanosheet onto the ITO surface (a) and total dissociation energy of Ti–O bonds that needs to be cleaved along the [01] (b), [10] (c), and [11] (d) axes of the $Ti_{0.87}O_2^{0.52-}$ nanosheet plotted as a function of the length of short side of the rectangular nanosheet. It is assumed that the nanosheet shape is rectangular (ratio of long side to short side is 0.38/0.30) and the nanosheet splits along each axis into two parts of identical shape (inset).

The above calculation can be applied to predict the threshold of the lateral size of various 2D nanosheets for their scission by changing the parameters including crystal structure, bond dissociation energy, and surface free energy of 2D nanosheets. For example, the threshold for scission of graphene, MoS_2 nanosheets, and $Ca_2Nb_3O_{10}^-$ nanosheets was estimated to be 600, 470, and 760 nm, respectively (Table S1, Supporting Information). Actually, we observed that the $Ca_2Nb_3O_{10}^-$ nanosheet with a size range of 5–10 μm was sectioned into smaller nanosheets (Figure S3, Supporting Information).

As shown in Figure 2f, the crevices running within a nanosheet tend to be orthogonal to each other at their intersections and perpendicular to the edge of the nanosheet, suggesting that the 2D rectangular lattice of the $Ti_{0.87}O_2^{0.52-}$ nanosheets is reflected. Then, we examined the in-plane orientation of $Ti_{0.87}O_2^{0.52-}$ nanosheets adsorbed on the polished flat ITO surface by acquiring low energy electron diffraction (LEED) patterns obtained from each nanosheet observed by low energy electron microscopy (LEEM).[55] As shown in **Figure 6**a, the obtained LEEM image shows monolayer tiling of the nanosheets, which is similar to the SEM image shown above (Figure 2a). The samples on the polished flat ITO surface gave recognizable LEED patterns (Figure 6b–f), although the spots were relatively broad. There are several possible explanations for the observed broad spots, for example, deterioration of crystallinity upon exfoliation or coverage with organic substances from the environment.

Since sharp spots can be observed by selected area electron diffraction (SAED) from the nanosheet with a high energy electron beam (e.g., 100 keV) as reported in our previous papers,[42,56,57] the possibility of the deterioration of crystallinity can be excluded. The most likely reason may be the coverage with organic substances on the nanosheets, which is often observed in LEEM/LEED measurements.[58] Since the acceleration energy for acquiring the LEED patterns is 30 eV, the penetration depth of electron beam is estimated to be ~1 nm,[59] which may not be enough to induce full diffraction by the nanosheets through the organic substances. The observed spots showed a *d*-value of 0.374 nm, which can be indexed as 10 and $\bar{1}0$ for the 2D rectangular unit cell of $Ti_{0.87}O_2^{0.52-}$ nanosheets. It is to be noted that the 100 reflection is extinct because of the face-centered symmetry. However, the 1*k*0 diffuse rod has a significant scattering intensity with $k \neq 0$ in this 2D structure,[42] which can be detected in the present reflection detection mode. The LEED patterns taken at the different places within one nanosheet were similar to each other (Figure 6d,e), confirming the single crystalline nature of each nanosheet. The adjacent nanosheet showed different lateral alignment (Figure 6b), due to the random azimuth orientation of different nanosheets as expected, and the two types of LEED patterns overlapped from the boundary region between the two nanosheets (Figure 6c). Furthermore, it was confirmed that the longer side of the rectangular nanosheet is parallel to the *c*-axis (Figure 6f), which is consistent with the fact that the mother layered crystal shows the largest growth along the *c*-axis direction.[42,43] Hence, it is strongly suggested that the observed crevices, which are perpendicular or parallel to the either edge of the rectangular nanosheet (Figure 2f), are parallel to the *c*-axis ([01] axis) or *a*-axis ([10] axis). This is consistent with the calculated results shown above (Figure 5).

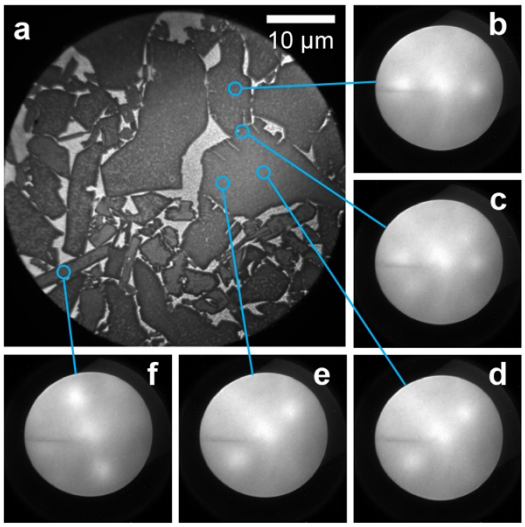

Figure 6. a) LEEM image of $Ti_{0.87}O_2^{0.52-}$ nanosheets on a polished flat ITO surface. b–f) LEED patterns acquired at an acceleration energy of 30 eV for each area designated by a blue circle (the diameter ~ 2 μm).

We also attempted to directly clarify the crystal orientation of crevices by acquiring LEED patterns. Although similar crevices running within a nanosheet adsorbed on the unpolished bumpy ITO surface were also observed by LEEM (Figure S4a, Supporting Information), the LEED spots from the nanosheets (Figure S4b–f, Supporting Information) were further broadened compared to those from the nanosheets adsorbed on the flat ITO surface. The 10-fold larger roughness of the unpolished bumpy ITO surfaces may be responsible for the further broadening of the spots. Since each nanosheet is adsorbed on the unpolished ITO substrate with conforming to its bumpy surface, the crystal plane of the nanosheet is tilted against the irradiated electron beam and its angle varies within a certain range, resulting in the broadened spots (Figure S5, Supporting Information). Due to this poorly-defined and extremely broad diffraction pattern, it was difficult to precisely confirm the crystal orientation of crevices by the LEED measurements.

The above calculations (Figure 5) suggest that the nanosheet cannot be sectioned when smaller than a certain value. To examine this hypothesis, we studied whether $Ti_{0.87}O_2^{0.52-}$ nanosheets with the lateral size ranging 200–1000 nm are sectioned upon adsorption on an unpolished bumpy ITO surface via the spin-coating. Since the crevices were hardly recognized in the small $Ti_{0.87}O_2^{0.52-}$ nanosheets not only on the flat ITO surface but also on the bumpy ITO surface (**Figure 7**a,b), we estimated the average size of the nanosheets on each substrate surface to examine if the nanosheets were sectioned. The area of the nanosheet was calculated using ImageJ software[60] based on the SEM images, and the size of the nanosheets was obtained by converting the calculated area into the length of one side of a square nanosheet with the same area. The average size of the nanosheets was estimated to be 439 ± 148 nm (n = 340) and 361 ± 132 nm (n = 280) on the flat and bumpy ITO surfaces, respectively, by taking the actual surface area (1.14 times larger than the projected area for the bumpy ITO surface) into account. The size distribution for the nanosheets on the flat ITO surface can be considered to be the original one contained in the nanosheet suspension. In the nanosheet size range of 300–400 nm on the bumpy ITO surface, the abundance ratio was comparable to that on the flat ITO surface (Figure 7c). In the ranges of 400–500 nm and larger, on the other hand, the abundance ratios of the nanosheets on the bumpy surface were smaller than the respective ratios of the nanosheets on the flat surface. It is considered that a

part of such large nanosheets were cut into smaller pieces upon adsorption on the bumpy surface. This can be supported by the fact that the abundance ratios in the ranges of 200–300 nm and below on the bumpy surface were larger than the respective ratios of the nanosheets on the flat surface. On the basis of these results, it was confirmed that the nanosheets are not sectioned when smaller than a certain value.

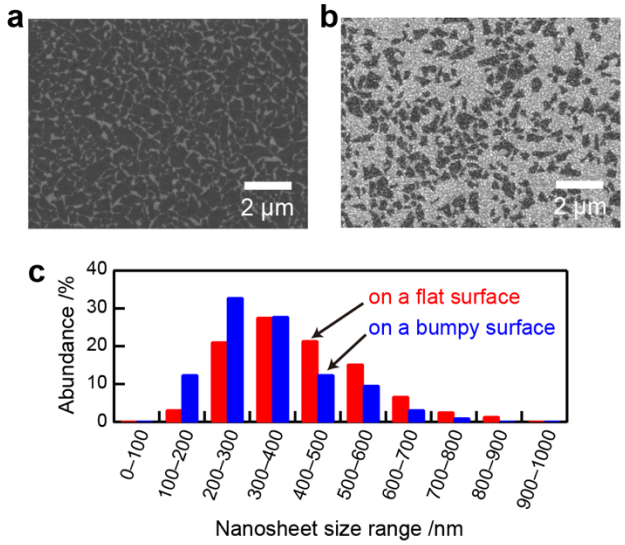

Figure 7. SEM images of small $Ti_{0.87}O_2^{0.52-}$ nanosheets spin-coated on a) polished flat and b) unpolished bumpy ITO surfaces. c) Size distribution of the nanosheets on the ITO surfaces.

Finally, we examined the behavior of the nanosheets upon adsorption on substrate surfaces via an electrostatic adsorption method.[39] When a bumpy ITO substrate coated with a cationic polymer was immersed into an aqueous suspension of the $Ti_{0.87}O_2^{0.52-}$ nanosheets, the nanosheets were adsorbed on the substrate surface due to electrostatic attraction. We observed various forms of the adsorbed nanosheets: torn, wrinkled, folded, and unsectioned (Figure S6, Supporting Information), which are different from the adsorption behavior via the spin-coating method shown above. In the case of the electrostatic adsorption method, the nanosheets can take various configurations in their suspension owing to their high flexibility, and contact to the substrate surface in various fashions. In the case where the two opposite edges of the nanosheet first adsorb on the substrate, the nanosheet would be torn when the length of the nanosheet between the two adsorbed points is shorter than that of the substrate surface along its bumpy surface. Conversely, if the length of the nanosheet is longer than that of the substrate surface between the two adsorbed points, the nanosheet may experience the compressive stress, resulting in the formation of wrinkles within the nanosheet, which is similar to the case where various 2D nanosheets are wrinkled upon mechanical

compression.[20–25] While the nanosheet can be torn under the tensile stress large enough to break the chemical bonds within the nanosheet, the compressive stress can be released by forming the wrinkles owing to high flexibility[45,56] as much as that the nanosheet can be folded. In contrast, in the case where the nanosheet is gradually adsorbed on the substrate surface from one edge of the nanosheet to the opposite edge to conform to the surface morphology of the substrate, the nanosheet would not be sectioned even on the bumpy surface because the tensile stress does not work. Hence, for the orthogonal scission of the nanosheets shown above (Figure 2f), it is important to employ the spin-coating method or equivalent methods so that the nanosheet stays flat at the surface of the solvent and then many parts of a single nanosheet simultaneously contact multiple summits of the randomly aligned bumps of the substrate surface to induce the isotropic tensile stress along the lateral direction of the nanosheets.

3. Conclusion

We have shown that the $Ti_{0.87}O_2^{0.52-}$ nanosheets can be sectioned into substantially rectangular-shaped fragments upon physical adsorption on a substrate with a nonflat surface via a spin-coating method. Upon adsorption on the bumpy surface, the tensile stress based on the integrated intermolecular forces acting between the nanosheet and the substrate surface isotropically works in the lateral direction of the nanosheets. Due to the high 2D anisotropy, the integrated intermolecular forces are large enough to cleave all the chemical bonds across one lattice plane perpendicular to the lateral direction of the nanosheets, leading to the scission of the nanosheets. The resultant crevices within the nanosheet preferentially run along the crystallographic orientation because of the smaller total dissociation energy of Ti–O bonds. In addition, the scission was attained for all the large nanosheets on the substrate surface. The principle to section the $Ti_{0.87}O_2^{0.52-}$ nanosheets presented here would also be applicable to not only 2D materials with other compositions and structures but also 1D anisotropic materials such as nanotubes and nanowires, offering a new processing technique for nanomaterials at a large scale.

4. Experimental Section

Reagents and Materials: All chemicals were of analytical grade and used as purchased. Milli-Q filtered water was used throughout the experiments. Si (100) wafers with a polished surface (Ra = 0.060 nm) and unpolished ITO (220 nm thick)-coated glass plates were

purchased from Furuuchi Chemical Co., Japan. Polished ITO (180 nm thick)-coated glass plates with a relatively flat surface were obtained from Kuramoto Co., Japan.

Preparation of the Titania Nanosheet Suspension: A colloidal suspension of $Ti_{0.87}O_2^{0.52-}$ nanosheets was prepared according to a previously reported procedure.[26,34,61] Lepidocrocite-type layered titanate, $K_{0.8}Ti_{1.73}Li_{0.27}O_4$, was synthesized by heating a stoichiometric mixture of TiO_2, K_2CO_3, and Li_2CO_3 powders at 1000 °C for 20 h. The obtained polycrystalline sample of $K_{0.8}Ti_{1.73}Li_{0.27}O_4$ was treated with 1 M HCl solution at ambient temperature for 72 h to yield a protonated phase, $H_{1.07}Ti_{1.73}O_4 \cdot H_2O$. The obtained $H_{1.07}Ti_{1.73}O_4 \cdot H_2O$ was dispersed in a TBA hydroxide solution ($TBA^+/H^+ = 1$) and shaken intermittently (10 strokes per day, manually) for a period of 1 month or agitated continuously (180 rpm, mechanically) for 1 week to be exfoliated. The resulting aqueous suspensions contained unilamellar nanosheets of $Ti_{0.87}O_2^{0.52-}$ with a lateral size of tens of micrometers (large $Ti_{0.87}O_2^{0.52-}$) and several hundred nanometers (small $Ti_{0.87}O_2^{0.52-}$) for intermittent and continuous shaking, respectively.

Solvent Replacement: The aqueous suspensions of $Ti_{0.87}O_2^{0.52-}$ nanosheets were subjected to centrifugation (1500 rpm, 420*g*) to remove an unexfoliated residue and/or restacked nanosheets, and then the top solution was collected and further centrifuged at 10000 rpm (9300*g* for large $Ti_{0.87}O_2^{0.52-}$) or 15000 rpm (21000*g* for small $Ti_{0.87}O_2^{0.52-}$) for 30 min. The resulting sediment was dispersed in DMSO to obtain the suspensions of $Ti_{0.87}O_2^{0.52-}$ nanosheets. The mass concentration of the nanosheets suspended in DMSO was estimated by the absorbance of the suspension diluted with DMSO, molar absorption coefficient, and density of DMSO (ρ = 1.10 g cm^{-3}). The molar absorption coefficient (ε) was determined by the combination of spectroscopic analysis and gravimetric quantification of the solid content upon heating at 1000 °C: $\varepsilon = 1.12(1) \times 10^4$ ($n = 3$) and $1.33(1) \times 10^4$ ($n = 2$) mol^{-1} dm^3 cm^{-1} at 270 nm for the large and small $Ti_{0.87}O_2^{0.52-}$ nanosheets suspended in DMSO, respectively. This value is similar to that of $Ti_{0.87}O_2^{0.52-}$ nanosheets suspended in water before solvent replacement: $\varepsilon = 1.09(0) \times 10^4$ ($n = 2$) and $1.32(1) \times 10^4$ ($n = 2$) mol^{-1} dm^3 cm^{-1} at 269 nm for aqueous suspensions of the large and small $Ti_{0.87}O_2^{0.52-}$ nanosheets, respectively.

Film Fabrication via Spin-Coating: Si wafers, unpolished ITO substrates, and flat ITO substrates (15 mm × 15 mm) were cleaned with acetone and then treated with oxygen plasma by using plasma ion bombardment (PIB-20, Vacuum Device, Japan) to turn their surface hydrophilic. The cleaned hydrophilic substrate was placed onto the sample holder of a spin coater (MS-B100, Mikasa, Japan) and covered with the nanosheet suspension in DMSO (60 μL) at adjusted concentrations (0.1–0.3 wt%). After standing for 30 s, the substrate was

rotated at the designated speed (1400–3000 rpm) for a certain period of time until the substrate surface was dried. Although we needed to adjust the rotation speed in response to the varied viscosity at different concentrations to form a monolayer tiling of the nanosheets, there were no significant differences in the shape of the sectioned nanosheets on the bumpy ITO surfaces.

Electrostatic Adsorption of Nanosheets: The large $Ti_{0.87}O_2^{0.52-}$ nanosheets were adsorbed on an unpolished ITO surface via the sequential adsorption procedure.[39] The cleaned hydrophilic ITO substrate was immersed in a polydiallyldimethylammonium (PDDA) chloride solution (20 g dm^{-3}, pH 9) to turn the surface positively charged. Subsequently, the PDDA-coated substrate was immersed in an aqueous suspension of $Ti_{0.87}O_2^{0.52-}$ nanosheets (0.06 g dm^{-3}, pH 9). The substrate was immersed in each solution for 20 min and then rinsed thoroughly with ultrapure water.

Apparatus: AFM images were collected in tapping mode using a scanning probe microscope (E-sweep, Hitachi High-Tech Science, Japan) equipped with a cantilever (SI-DF20). In-plane XRD measurements were performed using synchrotron X-ray radiation (λ = 0.11991(2) nm) at BL-6C, Photon Factory, High Energy Accelerator Research Organization (KEK). A field emission SEM (JSM-7001F, JEOL, Japan) with a Schottky electron gun was employed to acquire SEM images at an acceleration voltage of 5 kV. LEEM (LEEM III, ELMITEC, Germany) with a background pressure of ~5×10^{-7} Pa was used to collect LEEM images and corresponding LEED patterns taken at acceleration energies of 0.3–0.4 eV and 30 eV, respectively. The obtained LEED pattern is rotated at ~188 degrees clockwise against the LEEM image due to the difference in the exciting current of the lens for the observation of LEEM images and acquisition of LEED patterns. Prior to the LEEM/LEED experiments, the samples were irradiated with UV light (λ < 300 nm, 1 mW/cm^2) in air for 8 h and irradiated with UV light (3 mW/cm^2) in an ultrahigh vacuum chamber overnight to remove the organic species on the sample surface by the photocatalytic ability of the $Ti_{0.87}O_2^{0.52-}$ nanosheets,[37,62,63] although the sample surface did not reach a completely clean condition due to the high load of contaminants from the atmosphere in the sample preparation chamber. A UV–vis spectrophotometer (V-670, Jasco, Japan) was used to record absorption spectra of nanosheet suspensions. Contact angles were measured by a contact angle meter (DMe-210, Kyowa Interface Science, Japan). We used water and methylene iodide for the contact angle measurements of the nanosheet and ITO surfaces to estimate their surface free energies. The surface free energies of the liquids were given as γ_L^d = 21.8, γ_L^h = 51.0, and γ_L = 72.8 mJ/m^2 for water and γ_L^d = 49.5, γ_L^h = 1.3, and γ_L = 50.8 mJ/m^2 for methylene iodide.[52]

Supporting Information

Supporting Information is available from the Wiley Online Library or from the author.

Acknowledgements

This work was partly supported by the World Premier International Research Center Initiative on Materials Nanoarchitectonics (WPI-MANA), MEXT, Japan, and CREST of the Japan Science and Technology Agency (JST) Grant Number JPMJCR17N1, Japan. We thank Takayuki Kikuchi and Dr. Yasuo Ebina (NIMS) for the supply of $Ti_{0.87}O_2^{0.52-}$ and $Ca_2Nb_3O_{10}^-$ nanosheets. The in-plane XRD measurements were performed under the approval of the Photon Factory Program Advisory Committee (Proposal No. 2020G503). N.S. acknowledges support from JSPS KAKENHI Grant Number 18H03869.

Conflict of Interest

The authors declare no conflict of interest.

Received: ((will be filled in by the editorial staff))
Revised: ((will be filled in by the editorial staff))
Published online: ((will be filled in by the editorial staff))

References

[1] A. K. Geim, K. S. Novoselov, *Nat. Mater.* **2007**, *6*, 183.

[2] M. Osada, T. Sasaki, *J. Mater. Chem.* **2009**, *19*, 2503.

[3] R. Ma, T. Sasaki, *Acc. Chem. Res.* **2015**, *48*, 136.

[4] R. Uppuluri, A. S. Gupta, A. S. Rosas, T. E. Mallouk, *Chem. Soc. Rev.* **2018**, *47*, 2401.

[5] C. Tan, X. Cao, X.-J. Wu, Q. He, J. Yang, X. Zhang, J. Chen, W. Zhao, S. Han, G.-H. Nam, M. Sindoro, H. Zhang, *Chem. Rev.* **2017**, *117*, 6225.

[6] M. Chhowalla, H. S. Shin, G. Eda, L.-J. Li, K. P. Loh, H. Zhang, *Nat. Chem.* **2013**, *5*, 263.

[7] K. S. Novoselov, A. Mishchenko, A. Carvalho, A. H. Castro Neto, *Science* **2016**, *353*, aac9439.

[8] J. Bai, X. Zhong, S. Jiang, Y. Huang, X. Duan, *Nat. Nanotechnol.* **2010**, *5*, 190.

[9] M. E. Schmidt, T. Iwasaki, M. Muruganathan, M. Haque, H. V. Ngoc, S. Ogawa, H. Mizuta, *ACS Appl. Mater. Interfaces* **2018**, *10*, 10362.

[10] K. Kim, M. Yankowitz, B. Fallahazad, S. Kang, H. C. P. Movva, S. Huang, S. Larentis, C. M. Corbet, T. Taniguchi, K. Watanabe, S. K. Banerjee, B. J. LeRoy, E. Tutuc, *Nano Lett.* **2016**, *16*, 1989.

[11] Y. Cao, J. Y. Luo, V. Fatemi, S. Fang, J. D. Sanchez-Yamagishi, K. Watanabe, T. Taniguchi, E. Kaxiras, P. Jarillo-Herrero, *Phys. Rev. Lett.* **2016**, *117*, 116804.

[12] J. Quan, L. Linhart, M.-L. Lin, D. Lee, J. Zhu, C.-Y. Wang, W.-T.; Hsu, J. Choi, J. Embley, C. Young, T. Taniguchi, K. Watanabe, C.-K. Shih, K. Lai, A. H. MacDonald, P.-H. Tan, F. Libisch, X. Li, *Nat. Mater.* **2021**, *20*, 1100.

[13] L. Wang, E.-M. Shih, A. Ghiotto, L. Xian, D. A. Rhodes, C. Tan, M. Claassen, D. M. Kennes, Y. Bai, B. Kim, K. Watanabe, T. Taniguchi, X. Zhu, J. Hone, A. Rubio, A. N. Pasupathy, C. R. Dean, *Nat. Mater.* **2020**, *19*, 861.

[14] C. Zeng, J. Zhong, Y.-P. Wang, J. Yu, L. Cao, Z. Zhao, J. Ding, C. Cong, X. Yue, Z. Liu, Y. Liu, *Appl. Phys. Lett.* **2020**, *117*, 153103.

[15] E. Y. Andrei, A. H. MacDonald, *Nat. Mater.* **2020**, *19*, 1265.

[16] S. R. Na, X. Wang, R. D. Piner, R. Huang, C. G. Willson, K. M. Liechti, *ACS Nano* **2016**, *10*, 9616.

[17] J.-H. Lee, D.-W. Jang, S.-G. Hong, B. C. Park, J.-H. Kim, H.-J. Jung, S.-B. Lee, *Carbon* **2017**, *118*, 475.

[18] M. Chen, Z. Wang, X. Ge, Z. Wang, K. Fujisawa, J. Xia, Q. Zeng, K. Li, T. Zhang, Q. Zhang, M. Chen, N. Zhang, T. Wu, S. Ma, G. Gu, Z. Shen, L. Liu, Z. Liu, M. Terrones, L. Wei, *Matter* **2020**, *2*, 666.

[19] T. Sakorikar, M. K. Kavitha, P. Vayalamkuzhi, M. Jaiswal, *Sci. Rep.* **2017**, *7*, 2598.

[20] D. A. Kunz, P. Feicht, S. Gödrich, H. Thurn, G. Papastavrou, A. Fery, J. Breu, *Adv. Mater.* **2013**, *25*, 1337.

[21] A. Castellanos-Gomez, R. Roldán, E. Cappelluti, M. Buscema, F. Guinea, H. S. J. van der Zant, G. A. Steele, *Nano Lett.* **2013**, *13*, 5361.

[22] A. V. Thomas, B. C. Andow, S. Suresh, O. Eksik, J. Yin, A. H. Dyson, N. Koratkar, *Adv. Mater.* **2015**, *27*, 3256.

[23] P. Kumar, K. V. Agrawal, M. Tsapatsis, K. A. Mkhoyan, *Nat. Commun.* **2015**, *6*, 7128.

[24] P.-Y. Chen, M. Liu, Z. Wang, R. H. Hurt, I. Y. Wong, *Adv. Mater.* **2017**, *29*, 1605096.

[25] H. Kim, J. Kee, D.-R. Seo, Y. Lee, C. W. Ahn, J. Koo, *ACS Appl. Mater. Interfaces* **2020**, *12*, 42294.

[26] T. Maluangnont, K. Matsuba, F. Geng, R. Ma, Y. Yamauchi, T. Sasaki, *Chem. Mater.* **2013**, *25*, 3137.

[27] N. Miyamoto, T. Nakato, *J. Phys. Chem. B* **2004**, *108*, 6152.

[28] R. Garcia, A. W. Knoll, E. Riedo, *Nat. Nanotechnol.* **2014**, *9*, 577.

[29] H. Li, Z. Ying, B. Lyu, A. Deng, L. Wang, T. Taniguchi, K. Watanabe, Z. Shi, *Nano Lett.* **2018**, *18*, 8011.

[30] Y. Saito, J. Ge, K. Watanabe, T. Taniguchi, A. F. Young, *Nat. Phys.* **2020**, *16*, 926.

[31] X.-D. Chen, W. Xin, W.-S. Jiang, Z.-B. Liu, Y. Chen, J.-G. Tian, *Adv. Mater.* **2016**, *28*, 2563.

[32] J. N. Israelachvili, *Intermolecular and Surface Forces*, Elsevier, Burlington, MA **2011**.

[33] T. Sasaki, M. Watanabe, H. Hashizume, H. Yamada, H. Nakazawa, *J. Am. Chem. Soc.* **1996**, *118*, 8329.

[34] T. Sasaki, M. Watanabe, *J. Am. Chem. Soc.* **1998**, *120*, 4682.

[35] F. Geng, R. Ma, A. Nakamura, K. Akatsuka, Y. Ebina, Y. Yamauchi, N. Miyamoto, Y. Tateyama T. Sasaki, *Nat. Commun.* **2013**, *4*, 1632.

[36] F. Geng, R. Ma, Y. Ebina, Y. Yamauchi, N. Miyamoto, T. Sasaki, *J. Am. Chem. Soc.* **2014**, *136*, 5491.

[37] L. Z. Wang, T. Sasaki, *Chem. Rev.* **2014**, *114*, 9455.

[38] T. Sasaki, M. Watanabe, *J. Phys. Chem. B* **1997**, *101*, 10159.

[39] T. Sasaki, Y. Ebina, T. Tanaka, M. Harada, M. Watanabe, G. Decher, *Chem. Mater.* **2001**, *13*, 4661.

[40] K. Akatsuka, M. Haga, Y. Ebina, M. Osada, K. Fukuda, T. Sasaki, *ACS Nano* **2009**, *3*, 1097.

[41] K. Matsuba, C. Wang, K. Saruwatari, Y. Uesusuki, K. Akatsuka, M. Osada, Y. Ebina, R. Ma, T. Sasaki, *Sci. Adv.* **2017**, *3*, e1700414.

[42] T. Sasaki, Y. Ebina, Y. Kitami, M. Watanabe, T. Oikawa, *J. Phys. Chem. B* **2001**, *105*, 6116.

[43] K. Fukuda, I. Nakai, C. Oishi, M. Nomura, M. Harada, Y. Ebina, T. Sasaki, *J. Phys. Chem. B* **2004**, *108*, 13088.

[44] K. Fukuda, Y. Ebina, T. Shibata, T. Aizawa, I. Nakai, T. Sasaki, *J. Am. Chem. Soc.* **2007**, *129*, 202.

[45] H. Sato, K. Ono, T. Sasaki, A. Yamagishi, *J. Phys. Chem. B* **2003**, *107*, 9824.

[46] L. Z. Wang, T. Sasaki, Y. Ebina, K. Kurashima, M. Watanabe, *Chem. Mater.* **2002**, *14*, 4827.

[47] N. Sakai, T. Sasaki, K. Matsubara, T. Tatsuma, *J. Mater. Chem.* **2010**, *20*, 4371.

[48] Y. Shi, M. Osada, Y. Ebina, T. Sasaki, *ACS Nano* **2020**, *14*, 15216.

[49] F. Kim, L. J. Cote, J. Huang, *Adv. Mater.* **2010**, *22*, 1954.

[50] Although the observed rectangular nanosheets have longer sides along the *c*-axis direction, we assumed that the short side of the rectangle is parallel to *c*-axis to make the calculation simpler.

[51] S. P. Koenig, N. G. Boddeti, M. L. Dunn, J. S. Bunch, *Nat. Nanotechnol.* **2011**, *6*, 543.

[52] D. K. Owens, R. C. Wendt, *J. Appl. Polym. Sci.* **1969**, *13*, 1741.

[53] H. L. Clever, C. C. Snead, *J. Phys. Chem.* **1963**, *67*, 918.

[54] Y.-R. Luo, *Comprehensive Handbook of Chemical Bond Energies*, CRC Press, Boca Raton, FL **2007**.

[55] E. Bauer, *Rep. Prog. Phys.* **1994**, *57*, 895.

[56] T. Tanaka, Y. Ebina, K. Takada, K. Kurashima, T. Sasaki, *Chem. Mater.* **2003**, *15*, 3564.

[57] M. Ohwada, K. Kimoto, T. Mizoguchi, Y. Ebina, T. Sasaki, *Sci. Rep.* **2013**, *3*, 2801.

[58] Samples for LEEM/LEED experiments are usually heated at high temperature to make the surface clean. However, we were unable to do it because of possible phase transition of the nanosheets to anatase or rutile as well as possible softening of glass employed as a substrate.

[59] K. Kanaya, S. Okayama, *J. Phys. D: Appl. Phys.* **1972**, *5*, 43.

[60] C. A. Schneider, W. S. Rasband, K. W. Eliceiri, *Nat. Methods* **2012**, *9*, 671.

[61] T. Sasaki, F. Kooli, M. Iida, Y. Michiue, S. Takenouchi, Y. Yajima, F. Izumi, B. C. Chakoumakos, M. Watanabe, *Chem. Mater.* **1998**, *10*, 4123.

[62] T. Sasaki, Y. Ebina, K. Fukuda, T. Tanaka, M. Harada, M. Watanabe, *Chem. Mater.* **2002**, *14*, 3524.

[63] N. Sakai, Y. Ebina, K. Takada, T. Sasaki, *J. Am. Chem. Soc.* **2004**, *126*, 5851.

Table of Contents

Titania nanosheets can be sectioned into substantially rectangular-shaped fragments when adsorbed on a nonflat surface via a spin-coating method. The scission of the nanosheets is attained by the integrated intermolecular forces large enough to cleave the chemical bonds inside the nanosheets. The resultant crevices within the nanosheets preferentially run along the crystallographic orientation, offering a new processing technique for nanomaterials.

N. Sakai,* M. Suzuki, T. Sasaki

Scission of 2D Inorganic Nanosheets via Physical Adsorption on a Nonflat Surface